SPRINGER PROCEEDINGS IN PHYSICS 110

SPRINGER PROCEEDINGS IN PHYSICS

90 **Computer Simulation Studies in Condensed-Matter Physics XV**
Editors: D.P. Landau, S.P. Lewis, and H.-B. Schüttler

91 **The Dense Interstellar Medium in Galaxies**
Editors: S. Pfalzner, C. Kramer, C. Straubmeier, and A. Heithausen

92 **Beyond the Standard Model 2003**
Editor: H.V. Klapdor-Kleingrothaus

93 **ISSMGE**
Experimental Studies
Editor: T. Schanz

94 **ISSMGE**
Numerical and Theoretical Approaches
Editor: T. Schanz

95 **Computer Simulation Studies in Condensed-Matter Physics XVI**
Editors: D.P. Landau, S.P. Lewis, and H.-B. Schüttler

96 **Electromagnetics in a Complex World**
Editors: I.M. Pinto, V. Galdi, and L.B. Felsen

97 **Fields, Networks, Computational Methods and Systems in Modern Electrodynamics**
A Tribute to Leopold B. Felsen
Editors: P. Russer and M. Mongiardo

98 **Particle Physics and the Universe**
Proceedings of the 9th Adriatic Meeting, Sept. 2003, Dubrovnik
Editors: J. Trampetić and J. Wess

99 **Cosmic Explosions**
On the 10th Anniversary of SN1993J (IAU Colloquium 192)
Editors: J. M. Marcaide and K. W. Weiler

100 **Lasers in the Conservation of Artworks**
LACONA V Proceedings, Osnabrück, Germany, Sept. 15–18, 2003
Editors: K. Dickmann, C. Fotakis, and J.F. Asmus

101 **Progress in Turbulence**
Editors: J. Peinke, A. Kittel, S. Barth, and M. Oberlack

102 **Adaptive Optics for Industry and Medicine**
Proceedings of the 4th International Workshop
Editor: U. Wittrock

103 **Computer Simulation Studies in Condensed-Matter Physics XVII**
Editors: D.P. Landau, S.P. Lewis, and H.-B. Schüttler

104 **Complex Computing-Networks**
Brain-like and Wave-oriented Electrodynamic Algorithms
Editors: I.C. Göknar and L. Sevgi

105 **Computer Simulation Studies in Condensed-Matter Physics XVIII**
Editors: D.P. Landau, S.P. Lewis, and H.-B. Schüttler

106 **Modern Trends in Geomechanics**
Editors: W. Wu and H.S. Yu

107 **Microscopy of Semiconducting Materials**
Proceedings of the 14th Conference, April 11–14, 2005, Oxford, UK
Editors: A.G. Cullis and J.L. Hutchison

108 **Hadron Collider Physics 2005**
Proceedings of the 1st Hadron Collider Physics Symposium, Les Diablerets, Switzerland, July 4–9, 2005
Editors: M. Campanelli, A. Clark, and X. Wu

109 **Progress in Turbulence 2**
Proceedings of the iTi Conference in Turbulence 2005
Editors: M. Oberlack et al.

110 **Nonequilibrium Carrier Dynamics in Semiconductors**
Proceedings of the 14th International Conference, July 25-29, 2005, Chicago, USA
Editors: M. Saraniti, U. Ravaioli

Volumes 64–89 are listed at the end of the book.

M. Saraniti U. Ravaioli
(Eds.)

Nonequilibrium Carrier Dynamics in Semiconductors

Proceedings of the
14th International Conference,
July 25–29, 2005, Chicago, USA

With 223 Figures

Springer

Professor M. Saraniti
Department of Electrical
and Computer Engineering
Illinois Institute of Technology
Suite 103, Siegel Hall
3301 South Dearborn Street
Chicago, IL 60616, USA

Professor U. Ravaioli
Institute for Advanced Science and Technolgy
University of Illinois
405 Nroth Mathes Avenue
Urbana, IL 61801, USA

Published in association with Canopus Publishing Limited, Bristol, UK

ISSN 0930-8989

ISBN-10 3-540-36587-7 Springer Berlin Heidelberg New York

ISBN-13 978-3-540-36587-7 Springer Berlin Heidelberg New York

Library of Congress Control Number: 2006929190

Springer is a part of Springer Science+Business Media.
springer.com

Printed in the UK

Cover concept: eStudio Calamar Steinen
Cover production: *design & production* GmbH, Heidelberg
Printing: Short Run Express, Exeter, UK

Printed on acid-free paper SPIN: 11575108 54/3141/mh 5 4 3 2 1 0

Preface

This volume contains invited and contributed papers of the 14th International Conference on Nonequilibrium Carrier Dynamics in Semiconductors (HCIS-14) held July 24-29, 2005 in Chicago, Illinois.

The conference featured five invited and 62 contributed talks, as well as 49 posters and an international contingent of more than 80 scientists. Following the tradition of the conference, the topics discussed identified the most promising developments of nonlinear transport studies. Among these, interesting contributions were offered on mesoscopic systems, coherence in charge transport, ultrafast phenomena and TeraHertz devices. Two sessions were devoted to high field transport in nitrides, while the discussion on spintronics and thermoelectric phenomena clearly indicated the importance of these topics for the next generations of devices. Finally, a session was devoted to molecular electronics and two to bioelectronics, stressing the interest of the community in the study of charge transport in complex macromolecular systems.

On behalf of the Program and International Advisory Committees, we thank the participants, who made the conference a successful and pleasant experience and the generous support of DARPA, IBM, the Beckman Institute of the University of Illinois, and the Illinois Institute of Technology in Chicago. We are also indebted to Ms. Sara Starkey and Ms. Carol Osmer for their invaluable contribution to the conference organization and administration.

Marco Saraniti
Umberto Ravaioli

Contents

Electron transport in curved low dimensional electron systems

N. Shaji[1*], H.Qin[1], I. Knezevic[1], C. Deneke[2], O.G. Schmidt[2], M. A. Eriksson[3] and R.H. Blick[1].

[1]Laboratory for Molecular-Scale Engineering, Electrical and Computer Engineering, University of Wisconsin-Madison, 1415 Engineering Drive, Madison, WI 53706, USA.

[2]Max-Plank-Institut für Festkörperforschung, Heisenbergstr. 1, D-70569 Stuttgart, Germany.

[3]Department of Physics, University of Wisconsin-Madison, 1150 University Avenue, Madison, WI 53706-1390.

Summary. To investigate geometric potentials in low dimensional electron systems, we have conducted first studies on topography dependant electron transport in complete tubes, using built in strain between lattice mismatched semiconductors. Initial studies reveal two regimes of electron transport which are probed by a varying perpendicular magnetic field. At low magnetic field, an increased zero field peak in magneto resistance followed by a negative magneto resistance is observed due to increase in electron scattering along curved regions. At high magnetic field, we find a linear increase in resistance of the curved region as compared to planar regions.

1. Introduction

Investigating electron transport in suspended low-dimensional electron systems is a new approach which allows us to study dissipation phenomena such as the interaction of single electrons with discrete phonon modes directly [1]. The next step is to suspend the electronic system and to change the topology and study curved and rolled up electron systems.

It has been shown theoretically that the confinement potentials of low dimensional systems with a mechanical degree of freedom can depend on their geometry [2, 3, 4]. Such non-planar systems combined with precision band engineering can be used to mechanically tune the required geometric confinement potential. This additional tuning of low dimensional systems

* Present Address: 2439 Engineering Hall, 1415 Engineering Drive, Madison, Wisconsin, 53706. Tel.: +1-608-213-0836; Fax: +1- 608-262-1952; e-mail: nakul@cae.wisc.edu.

through mechanical relief gives non-planar systems an advantage over its planar counterpart.

Starting from Ref [2], we see that similar to electron confinement via electrostatic gates in planar systems, geometrically confined potentials in non-planar systems can be modeled to first order as simple square well potentials. The binding energies of such non-planar systems are found to be inversely proportional to the square of curvature radius of the non-planar system. In addition such confinement potentials cause a phase shift in the electronic wave function propagating phase coherently through the system, corresponding to Berry's phase [5].

Confining a 2DEG in such curved and rolled geometries marks the first step to obtaining a non-planar low dimensional electron system. First studies performed by peeling a planar hall bar off the supporting substrate and attaching it to curved geometries have shown that the magneto-resistance oscillations in millimeter sized bent electron gases depend on the dispersion of Landau levels and a cosine variation of linear resistance [6]. To obtain tubular geometries with smaller diameters, we make use of the built-in strain in heterostructures. When lattice mismatched semiconductors are grown layer by layer epitaxially, a strain is built in as the epitaxial layer tries to align its lattice with that of the substrate. Release of this strain by removing the sacrificial layer below the strained bilayer causes the bilayer to bend forming tubular geometries as shown in Fig. 1(a) [7, 8]. Recent experiments on tubes formed from such strained 2DEG structures [9] have shown a wash out of magneto-resistance oscillations with tube formation.

2. Experiment

The heterostructure we report on consists of a transport layer formed by 10 nm GaAs cap layer followed by 10 nm $Al_{0.33}Ga_{0.67}As$, 2 nm GaAs (silicon delta doped), 20 nm $Al_{0.33}Ga_{0.67}As$, 20 nm GaAs quantum well (2DEG). The strained bilayers following the transport layer consists of 20 nm $Al_{0.33}Ga_{0.67}As$, 14 nm $In_{0.2}Ga_{0.8}As$ (strained) and 10 nm AlAs (sacrificial layer) over a GaAs substrate. Since $In_{0.2}Ga_{0.8}As$ has a larger lattice constant, the layers curve up to form the tube when the strain is released by removing the sacrificial layer of AlAs.

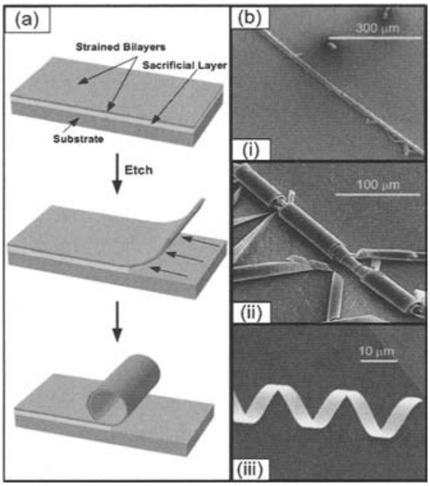

Fig. 1. (a) The built-in strain between mismatched semiconductors is released by removing the sacrificial layer below it. Tube rolls upwards as InGaAs has larger lattice constant than AlGaAs. (b) Fabricated tubes (i) 720 µm long single turn tube. (ii) Multi turn tube. (iii) Spiral coils.

Fig. 1(b) shows the various types of tubes fabricated from this strained heterostructure. Single turn tubes as long as 720 µm were fabricated when the width of the mesa was equal to πD, where D is the tube diameter (i). To fabricate multi turn tubes the initial mesa was patterned to have a width much larger than πD, to perform multiple rotations when the strain is released (ii). When the initial width of the mesa was smaller than πD, the bilayer was unable to complete a single rotation, and instead would share its strain with nearby elements performing angular rotations which resulted in the formation of helical coils (iii).

A hall bar was fabricated to characterize electron transport through the sample. The mesa was a 150 µm square with leads 600 µm long and 60 µm in width. AuGe/Ni/AuGe ohmic contacts were annealed at 420 degrees celsius. The sample at 2K showed conduction only in the presence of light. With an applied back gate bias and a varying magnetic field applied perpendicular to the crystal surface, the sample showed a superposition of oscillations from parallel conducting channels. This is due to the photoconduction from 14nm InGaAs and through electron transport in the 2DEG. Similar magneto oscillations in thin slabs of InGaAs have been reported [10]. The extracted carrier sheet density for the 2DEG is $n_s = 3.8 \times 10^{14}$ m^{-2} and the mobility is 680 cm^2/Vs. Due to this low mobility, the electron transport through the sample was non-ballistic.

The sacrificial layer of AlAs was removed by dipping the mesa in 1% HF. Upon releasing the strain the leads curved up to form tubes. Due to the length of the leads being much larger than the tube diameter and being pinned down at one end by contacts, all the tubes did not survive this process, which limited us to taking two-point measurements.

The two point measurements on the planar sample shows an increase in resistance with applied magnetic field. A closer look at the low magnetic field region shows a giant magneto resistance at zero magnetic field and a negative magneto resistance region for fields less than 0.7T. Such peaks and negative resistance region in parallel conducting sample have been reported before [11] and a fit to theory suggests an interplay of weak localization in both 2DEG and bulk confinement.

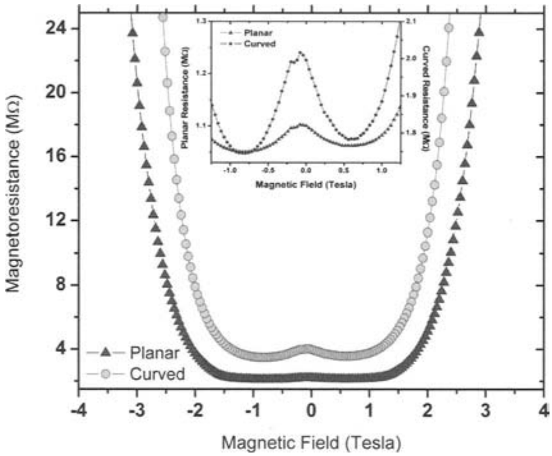

Fig. 2. Comparison of magneto-resistance variation in both planar and rolled up mesa. The inset shows the low magnetic field regime where a zero field peak and a negative magneto resistance region is seen in both planar and rolled mesa.

Upon tube formation, we see two regimes of electron transport (Fig 2). The inset of Fig. 2 shows the low magnetic field region where we see an unexpected increase in zero-field peak resistance from 52 kΩ to 260 kΩ indicating an additional scattering mechanism that is dominant in curved regions. A likely candidate for this scattering in curved region is surface scattering as we release a new InGaAs surface which was initially attached to the sacrificial layer. This release causes the formation of dangling bonds which now can scatter the electrons in curved regions.

At higher magnetic fields, there is a linear change in magneto-resistance as if there is a linear change in effective electronic width of the sample. A possible explanation is that at high fields, the resistance of the curved region is higher than in the planar region, and the linear change in overall *planar width* of the mesa is reflected in the linear increase in overall resistance. Proposals for this increase in resistance at curved regions include a change in local piezoelectric potential and confinement of carriers to locally bound states due to the geometry. More measurements are needed to confirm the exact nature reason of this behaviour.

We have shown clear topography induced changes in electron transport through a parallel conducting two dimensional electron systems. With better material engineering, a higher mobility 2DEG can be confined in these non-planar systems to probe pure ballistic electron transport. Incorporating larger strain in such systems would help realize tubular low dimensional geometries with smaller diameters useful for probing geometric potentials and achieving topographical quantum systems.

We thank ARO and NSF MRSEC for financial support.

References

1. Weig, E. M. et al.: 'Single-Electron-Phonon Interaction in a Suspended Quantum Dot Phonon Cavity', *Phys. Rev. Lett.*, **92**, 046804, 2004.
2. Chaplik, A. V. and Blick, R. H.: 'On geometric potentials in quantum-electromechanical circuits', *New J. Phys.*, **6**, 33, 2004.
3. da Costa, C. T.: 'Quantum mechanics of a constrained particle', *Phys. Rev. A.*, **23**, 1982–1987, 1981.
4. Foden, C. L. et al.: 'Quantum magnetic confinement in a curved two-dimensional electron gas', *J. Phys.: Condens. Matter.*, **6**, L127-L134, 1994.
5. Berry, M. V.: 'Quantal phase factors accompanying adiabatic changes', *Superlattices and Microstructures*, **33**, 347–35, 2003.
6. Lorke, A. et al.: 'Curved two-dimensional electron gases', *Phys. Rev. Lett.*, **92**, 046804, 2004.
7. Prinz, V. Ya. et al.: 'Free-standing and overgrown InGaAs/GaAs nanotubes, nanohelices and their arrays ', *Physica E.*, **6**, 828, 2000.
8. Schmidt, O. G. and Eberl, K.: 'Thin solid films roll up into nanotubes', *Nature*, **410**, 168, 2001.
9. Mendach, S. et al.: 'Preparation of curved two-dimensional electron systems in InGaAs/GaAs-microtubes', *Physica E.*, **23**, 274–279, 2004.
10. McElhinney, M. et al.: 'Quantum transport measurements on Si δ- and slab-doped In0.53Ga0.47As grown by molecular beam epitaxy ', *Journal of Crystal Growth*, **150**, 266, 1995.
11. Mace, D. R. et al.: 'Negative magnetoresistance in a parallel-conducting InGaAs structure', *J. Phys.: Condens. Matter.*, **4**, L487-L494, 1992.

Fabrication and Characterization of InAs Mesoscopic Devices

M. Koyama, M. Furukawa, H. Ishii, M. Nakai, T. Maemoto, S. Sasa, and M. Inoue

New Materials Research Center, Osaka Institute of Technology
5-16-1 Ohmiya, Asahi-ku, Osaka 535-8585, Japan

Summary. The transport properties of symmetry-broken InAs mesoscopic devices are reported. We fabricated InAs mesoscopic structures with a triangular anti-dot structure to serve as a ballistic rectifier. In this structure, rectification effects relying on the ballistic transport were observed at room temperature and 77K. These results show the superiority of InAs/AlGaSb heterostructures for the realization of ballistic mesoscopic devices.

1 Introduction

InAs-based heterostructures have various advantages, such as small effective mass and strong electron quantum confinement, for the realization of quantum effect devices. In addition, due to the long phase coherence time, InAs-based heterostructures offer the possibility to observe ballistic electron transport properties at relatively high temperatures compared to GaAs/AlGaAs heterostructures. Therefore, these material systems are suitable for the development of mesoscopic devices which rely on ballistic electron transport. As one of the typical sample of such applications, ballistic rectifiers are actively being researched these days. Based on the research of Song et al., it was thought that ballistic rectification is based on quasi-classical transport properties [1][2]. Fleischmann et al. reported the microscopic theoretical model with Landauer-Büttiker approach [3]-[5]. In this paper, we report on an InAs mesoscopic structure for a high temperature operation as a ballistic rectifier.

2 Fabrication

The epitaxial layer of the InAs/AlGaSb heterostructure was grown by molecular beam epitaxy on a semi-insulating GaAs(100) substrate. In order to improve the crystal quality of the InAs channel layer, an undoped 1.5 μm thick AlSb layer was grown as a buffer layer to accommodate the lattice mismatch of about 7% between GaAs and InAs. The heterostructure consists of an AlSb buffer layer, AlSb/GaSb superlattices, a 200 nm AlGaSb bottom barrier, an 8 nm AlSb barrier layer, a 15 nm InAs channel layer, a 15 nm AlGaSb upper barrier layer, and finally a 10 nm GaSb cap layer. Hall-effect measurements by the van der Pauw method showed electron mobility of 20,000 cm^2/Vs, sheet carrier density of 1.8×10^{12} cm^{-2} at 300K, and 140,000 cm^2/Vs, 1.0×10^{12} cm^{-2} at 77K, respectively.
An atomic force microscope image of the central part of the device is shown in the Fig. 1. Definition of the antidot and probes of device was achieved by electron beam lithography with ZEP-520A resist and wet chemical etching. The etchant was phosphoric acid based (H_3PO_4 : H_2O_2 : H_2O = 1 : 1: 100). Next, the Hall bridge was fabricated by photolithography. In order to eliminate the leakage current from the buffer layer, all regions except for the Hall bridge mesa were covered with SiO_2 insulator. Non-alloyed ohmic metals, In (20 nm)/Au (120 nm), were then deposited directly onto the InAs channel layer by thermal evaporation and were defined by lift-off. Metal pads for bonding were formed at the same time. The size of this device is as small as the open quantum dot structures in which we have observed ballistic transport properties and electron wave interference effects at 4.2K [6].

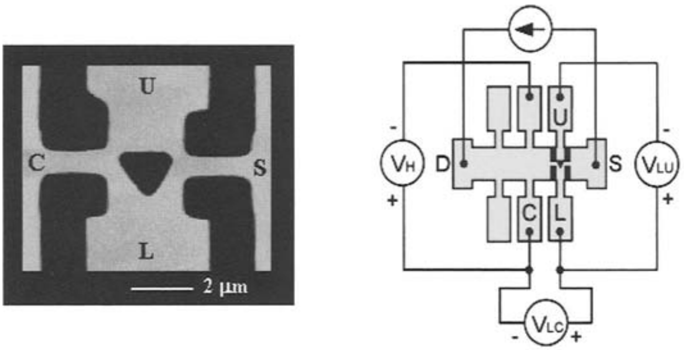

(a) AFM image (b) Measurement Configuration

Fig. 1 Atomic force microscope image of the central part of ballistic rectifier (a). The circuit diagram of the measurement system (b). DC current was applied between Drain and Source.

3 Experimental Results and Discussion

We measured the *I-V* characteristics at room temperature and 77K. Fig. 2 shows the output voltage (V_{LU}) as a function of input current (I_{DS}). For both temperatures, the output voltage V_{LU} shows negative polarity despite of the I_{DS} polarity. Therefore, a rectification effect was observed for both temperatures. As shown in the Fig. 2 (a), the stronger effect was observed at 77K probably due to the increased mean free path of about 2 μm. We believe that these characteristics reflect the ballistic transport in InAs. Although negative V_{LU} was observed on reversal of the drain-source current, the magnitude of V_{LU} shows asymmetry with respect to $I_{DS} = 0$. This result implies the asymmetry of the triangular anti-dot and the distances between the dot and source or drain wires. The distance between the reservoir and source or drain wire may also affect the characteristics. (From Fig. 1 (a), the left wire is slightly misaligned upward with respect to the triangular anti-dot.) Therefore, it is likely that the injection ratio of electrons toward probe U from the left wire is larger than that from right wire.
Figure 2 (b) shows the logarithmic plot of the I_{DS}-V characteristics for $I_{DS} >$ 0 measured at 77K. The V_{LU} shows nonlinear characteristics due to the rectification effect while V_{LC} follows Ohm's low. Compared to GaAs/AlGaAs, the nonlinear effect in InAs persists for I_{DS} well above 100 μA indicating the superiority of InAs device. V_H is the reference voltage

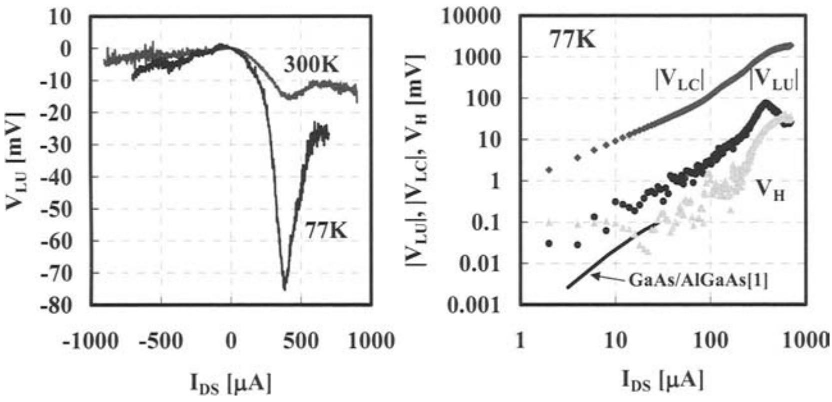

(a) The output voltage versus input direct current

(b) Logarithmic plot of the *I-V* characteristics

Fig. 2 The output voltage (V_{LU}) as a function of input direct current (I_{DS}) measured at room temperature and 77K (a). Logarithmic plot of the *I-V* characteristics measured at 77K.

measured across the channel and outside the left wire (Fig. 1 (b)). Comparing V_{LU} and V_H, the polarity of each voltage is opposite. Therefore, V_{LU} was not affected by the reference voltage V_H. However, for both temperatures, the rectification effects drastically decreased for $I_{DS} > 400$ μA. It is likely that the anti-collimation effect increased by increasing the applied voltage resulting in the increase in the propagation toward probe U.

4 Conclusion

We fabricated and characterized an InAs mesoscopic ballistic rectifier with a triangular anti-dot structure. Clear rectification characteristics were observed for both room temperature and 77K and persisted up to higher current level over 100 μA compared to GaAs/AlGaAs. These results show a potential for higher temperature operation ballistic rectifier by using InAs/AlGaSb heterostructure.

References

2. 1. Song, A. M. et al.: 'Non linear Electron Transport in an Asymmetric Microjunction: A Ballistic Rectifier', *Phys. Rev. Lett.*, **80**, 3831-3834, 1998.
2. Song, A. M.: 'Formalism of nonlinear transport in mesoscopic conductors', *Phys. Rev. B*, **59**, 9806-9809, 1999.
3. Fleischmann, R. and Geisel, T.: 'Mesoscopic Rectifiers Based on Ballistic Transport', *Phys. Rev. Lett.*, **89**, 016804, 2002.
4. Büttiker, M. and Sánchez, D.: 'Comment on "Mesoscopic Rectifiers Based on Ballistic Transport" ', *Phys. Rev. Lett.*, **90**, 119701-1, 2002.
5. Geisel, T. and Fleischmann, R.: 'Geisel and Fleischmann Reply', *Phys. Rev. Lett.*, **90**, 119702-1, 2002.
6. Maemoto, T. et al.: 'Magneto transport in an InAs/AlGaSb quantum wire with a weak periodic potential', *Physica B*, **272**, 110-113, 1999.

Nonlinear Effects on Quantum Interference in Electron Billiards

C. A. Marlow, R. P. Taylor, M. Fairbanks, and H. Linke

Physics Department, University of Oregon, Eugene OR 97403-1274, USA

Summary. Magnetoconductance fluctuations are used to study the effect of an applied bias on an electron billiard. At lower bias, nonlinear effects can be well described by electron heating alone, while at higher bias ($V > 2$mV, ~5% of the electron Fermi energy) non-equilibrium effects become significant. At high bias, we also observe that the spectral content of the MCF is sensitive to the nonequilibrium effects. Spectral behavior is consistent with a fractal scaling of the conductance fluctuations with magnetic field, resulting in the first observation of fractal conductance fluctuations outside of the linear regime of transport.

1 Introduction

In this work, we use electron quantum interference effects to study the effect of an applied bias on electron transport. The electron billiards used to study these effects were defined by e-beam lithography and wet etching of the two-dimensional electron gas (2DEG) formed in the GaInAs quantum well in the GaInAs/InP heterostructure (see Fig. 1(a)). A square (Figs. 1(b)) and rectangular (Fig. 1(c)) were studied with areas, after depletion, of 0.8 μm^2 and 3.4 μm^2, and Fermi energies of 35 meV and 38 meV, respectively. In both cases, the phase coherence length and mean free path were greater than the device dimensions resulting in phase-coherent, ballistic transport. Quantum interference effects lead to fluctuations in billiard conductance as a function of a perpendicular applied magnetic field, B. These magnetoconductance fluctuations, MCF, are a sensitive reproducible probe of the electron dynamics within the billiard[1] and will be used here to monitor the effect of an applied bias on electron transport.

In the presence of an applied bias, electrons are injected into the billiard with excess energy. If the electrons have time to thermalize before leaving the billiard, they relax through electron-electron scattering and the excess energy is distributed amongst the electrons in the billiard causing an increase in overall electron temperature inside the billiard. Previous experiments have found that for small applied bias voltages, in the μV range, the primary effect of the bias is electron heating.[2,3] The electron heating can be characterized by an effective temperature, $T_e(V)$, written:[2]

$$T_e(V) = \frac{T_L}{2} + \frac{1}{2}\sqrt{T_L^2 + e^{-\gamma\tau_\varepsilon(V)}\frac{3}{2\pi^2}\left(\frac{eV}{k}\right)^2} \quad (1)$$

where T_L is the temperature of the lattice, $\exp(-\gamma\tau_\varepsilon(V))$ is the fraction of electrons that thermalize before escaping the billiard, γ is the escape rate,[4] and $\tau_\varepsilon(V)$ is the electron-electron interaction time. At the temperatures used here phase-breaking is dominated by electron-electron scattering, so the experimentally measured phase breaking length, τ_ϕ, will be used for τ_ε when calculating $T_e(V)$. τ_ϕ was determined from the measured MCF using a well-established method that analyzes the correlation field of the fluctuations as a function of magnetic field.[5]

We use this heating model to study the importance of nonequillibrium effects in the mV range. MCF measurements were taken as a function of T and V and directly compared using Eq.1 to translate V to $T_e(V)$; any departure between the two behaviors we interpret as nonequilibrium effects.

2 Experimental Results

The two-terminal magnetoconductance through the billiards was measured as a function of a perpendicular B using a standard low frequency ac lock-in technique. In order to apply a bias across the billiard, a tuneable dc bias V was added to a small ac signal (rms amplitude 20 μV on order of the thermal energy $kT \approx 20$ μeV). Measurements were made at a range of temperatures with $V = 0$ mV and also for a range of dc biases (up to 3 mV) at $T = 230$ mK.

Figure 1(d) shows the MCF for the square billiard measured for a range of T (black curves) and V (gray curves). The bias values have been related to the associated temperature using Eq. 1. At low bias, the fluctuations taken at a bias are similar to those at the corresponding temperature $T_e(V)$, consistent with previous observations in GaAs/AlGaAs billiards[3] where agreement was seen in the μV range. At higher bias, however, a departure is seen between the MCF measured at V and those at the related T, indicating that at higher bias, the effect of the bias on the fluctuations is not just electron heating.

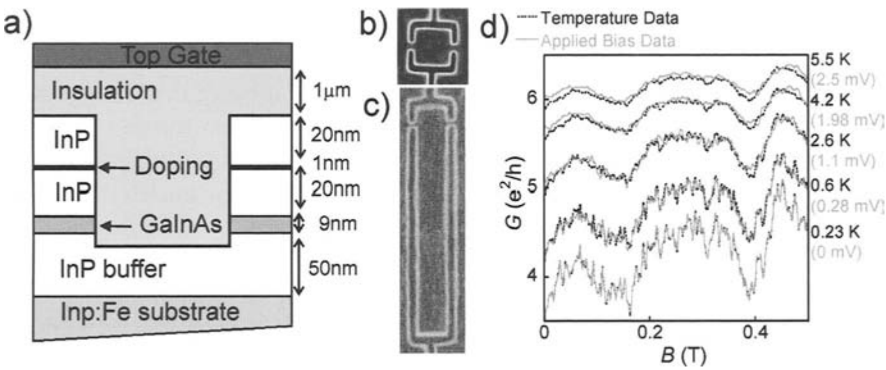

Fig. 1. a) Schematic representation of GaInAs/InP billiard system, scanning electron micrographs of the b) square and c) rectangular billiard and d) MCF for the square billiard, measured for a range of temperatures at zero bias (black curves) and range of bias at $T = 230$ mK (gray curves). Traces are offset for clarity.

We also investigate the effect of the bias on the spectral content of the fluctuations. The power spectrum, $S(f)$, of the MCF for the square billiard at $T = 0.6$ K and $V = 0$ mV is shown in Fig. 2(a). All MCF for the billiards presented here show $1/f^{\alpha}$ scaling, where $f = 1/\Delta B$ and α is the spectral exponent which characterizes the entire spectral content of the fluctuations. The α values observed indicate a fractal scaling[6] of the fluctuations consistent with previously observed fractal conductance fluctuations, FCF, in similar systems.[7]

Figures 2(b) and 2(c) show the dependence of the spectral exponent, α, on both T and T_e (V) for the square and rectangular billiard respectively. We see that α increases with increasing T, consistent with previous results.[7] The same increase is seen with increasing T_e (V). It appears, however, that at T_e $(V) \sim 4$ K, (corresponding to ~ 2 mV) the evolution of α with V departs significantly from that of α (T), confirming again that the bias is having an additional effect besides heating.

3 Discussion

The deviations of the characteristics of the MCF indicate that the effect of the high bias is nontrivial; the bias does not just increase electron energy, but instead changes electron dynamics within the billiard. Future work needs to experimentally investigate the precise role of nonequillibrium electrons in the generation of MCF.

The fractal nature of MCF has been observed to be is robust to changes in many system parameters.[7] The effect of the nonequillibrium electrons on the spectral exponent is unexpected. Future exploration of this dependence may provide insight into the origins of FCF. In addition, further analysis of FCF in the nonlinear region may help uncover the mechanisms responsible for the symmetry breaking of the spectral content of the FCF with respect to reversal of magnetic field seen previously.[8]

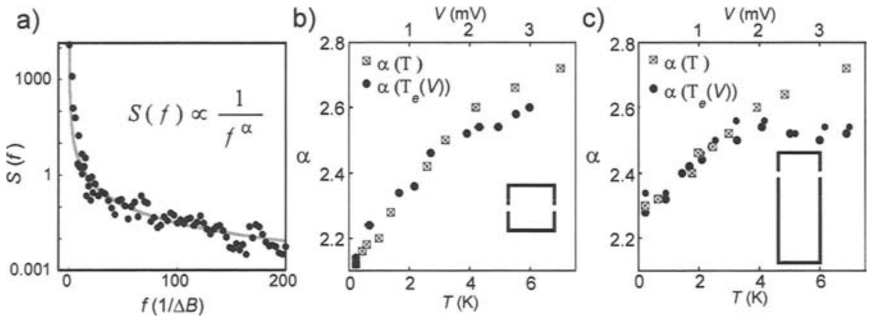

Fig. 2. a) Power spectra of MCF measured on square billiard (T = 0.6 K, V = 0 mV), spectral exponent α as a function of T and T_e (V) for b) square and c) rectangular billiard.

References

1. Beenakker, C. W. J. and van Houten, H.: 'Quantum transport in semiconductor structures', *Solid State Physics*, edited by H Ehrenreich and D Turnbull, Academic Press, **44**, 1991.
2. Linke, H. et al.: 'Non-equilibrium electrons in ballistic quantum dot', Phys. Stat. Sol., **204**, 318, 1997.
3. Switkes, M. et al.: 'High bias transport and magnetometer design in open quantum dots',Appl. Phy. Lett., **72**, 471, 1998.
4. Jensen, R. V.: 'Chaotic scattering, unstable periodic orbits, and fluctuations in quantum transport',Chaos, **1**, 101, 1991.
5. Bird, J. P. et al.:'Phase breaking in ballistic quantum dots: a correlation field analysis', Surf. Sci., **361/362**, 730, 1996.
6. Barnsley, M. F. et al.: *The Science of Fractal Images*, Springer-Verlag, 1988.
7. Micolich, A. P. et al.:'Three key questions on fractal conductance fluctuations: Dynamics, quantization, and coherence', Phys. Rev. B **70**, 085302, 2004; Marlow, C. A. et al.: submitted, 2005.
8. Marlow, C. A. et al.: to be submitted, 2005.

Prediction of Entanglement Detection by I-V Characteristics

T. Zibold[1], P. Vogl[1], A. Bertoni[2]

[1]Walter Schottky Institute, Technische Universität München, 85748 Garching, Germany
[2]National Research Center on "nanoStructures and bioSystems at Surfaces" (S3), INFM-CNR, 41100 Modena, Italy

Summary. We present a theoretical analysis of a ballistic GaAs/AlGaAs quantum device that allows the straightforward control and detection of the entanglement between an open, stationary double quantum wire system and a singly occupied electrostatically defined double quantum dot. The read-out involves the measurement of only the DC I-V characteristics.

1 Introduction

While there is no shortage in theoretical proposals for the creation of entangled qubits in semiconductors (see, e.g., [1,2,3,4]), the experimental realization of their write-in and read-out processes has proven to be extremely difficult, mostly because of the short coherence times and strong interactions between elementary excitations in solids [5]. Charge-based qubits have been proposed either based on double quantum dots (DQD) or electron wave packets propagating ballistically within two adjacent quantum wires (QWR) [6]. Recently, it has been pointed out that qubits or, more generally, quqits (quaternary state bits) can also be realized on the basis of stationary scattering states in open devices [7]. While these stationary wave functions cannot be normalized, the transmission and reflection play the role of the computational basis. The unitarity of ballistic scattering guarantees a well-defined Hilbert space. To the best of our knowledge, however, no concrete write-in and read-out processes for entangled quqits or qubits associated with stationary scattering states have been proposed so far.

We present a quantitative theoretical analysis of a concrete quantum transport device that allows the straightforward control and detection of the entanglement between an open, stationary QWR qubit based on a solid-state Mach-Zehnder interferometer and a DQD qubit. The read-out involves the measurement of only the DC $I-V$ characteristics, no higher order current correlations are required to detect entanglement.

2 Method and Results

Figure 1 shows a schematic top view of the proposed device consisting of two stacked GaAs/AlGaAs two-dimensional electron gases (2DEG). The Mach-Zehnder interferometer in dark gray is composed of two adjacent QWR that are coupled by two tunneling windows [8]. The latter act as rotation gates (R). Along the upper QWR, there is an adjustable barrier in between the rotation gates that acts as a tunable phase gate V_G. An electrostatically defined DQD (light gray) is located in a second 2DEG underneath the QWR layer. The tunnel coupling between the two quantum dots as well as their energy spectra are assumed to be controlled by external gates that are not shown [9]. By applying a bias voltage V equal to 50 μV between the upper left and the remaining three contacts, current flows predominantly from the upper left to the upper right contact (J_0) and from the upper left to the lower right contact (J_1), respectively, depending on the phase gate voltage V_G.

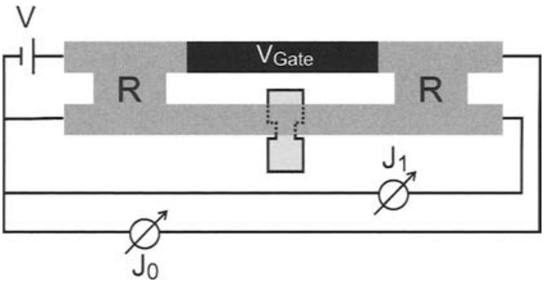

Fig. 1. Schematic top view of the proposed quantum transport device. The device is realized by two stacked GaAs/AlGaAs 2DEGs. The top 2DEG is depleted by external gates to form a Mach-Zehnder interferometer (dark gray). In the bottom 2DEG two coupled quantum dots (light gray) are located. For sake of clarity, the figure is not drawn on scale.

We have calculated the ballistic current through this 3D device, using a single-band effective mass description for the electronic Hamiltonian and by including the Coulomb interaction between the electrons in the QWR and the DQD non-perturbatively. To this end, we have extended the CBR method [10] to deal with Green's functions of two-particle Hamiltonians for distinguishable particles. After determination of the single-particle scattering states of the open QWR system and the eigenstates of the closed DQD system, the two-particle Hamiltonian is diagonalized in the basis of the product states, including the Coulomb interaction between the two subsystems. The single-particle basis states associated with the QWR are determined realistically from the retarded Green's function of the open device using our device simulator nextnano³. To simplify the two-electron problem, however, we have mapped the DQD subsystem onto a two-level tunneling Hamiltonian that is characterized by a tunnel coupling t in the range between 0 and 20 μeV and a bare splitting of $\Delta = 10$ μeV between the two levels [9]. The charge distribution of the electron in the DQD is approximated by two localized charge distributions that are weighted by the projections of the two-particle eigenstates onto the DQD basis states.

In the present calculations, we take both GaAs 2DEGs to be 10 nm thick; the vertical distance between the QWR and the DQD layer is set to 80 nm. Each of the quantum wires is 55 nm wide, 1000 nm long, and the lateral distance between them amounts to 20 nm. The rotation gates have a length of 85 nm. One of the quantum dots is located exactly beneath the center of the barrier region in between the 2 quantum wires. The lateral distance between the 2 quantum dots is chosen to be 60 nm. The Fermi energy has been set to 1.6 meV in the lowest subband. This causes the tunneling windows to act as almost perfect rotation gates for low bias voltage.

At first, we study the $I-V$ characteristics of the device for a situation where the tunneling between the quantum dots is inhibited ($t=0$). For $V_G = 0$, the rotation gates are dimensioned in such a way that interference causes the current between the upper left and right contact to be zero ($J_0 = 0$) and to attain a maximal value between the left top contact and the lower right contact ($J_1 = J_{max}$). Application of a finite voltage V_G to the phase gate results in DC currents J_0 and J_1 that have intermediate values between 0 and J_{max} and are phase-shifted by π relative to one another.

We now allow the dot electron to tunnel between the quantum dots. This leads to an entanglement of the QWR and the DQD. This entanglement puts the QWR subsystem into a mixed state which causes the interference through the upper and the lower wire to be suppressed. The degree of suppression can be characterized by the visibility v which we define by $v = \left[(J_1 - J_0)/(J_1 + J_0)\right]_{V_G=0}$. This quantity can be shown to be related to the von-Neumann entropy by $S = -\sum_{i=+,-} p_i \ln p_i$, where $p_\pm = \left(1 \pm v\right)/2$.

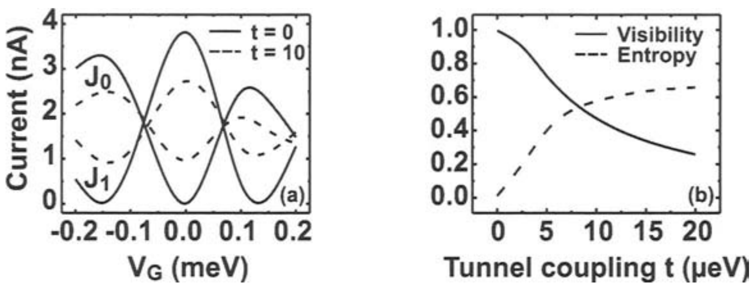

Fig. 2. (a) Currents J_0 and J_1 as a function of the gate voltage of the phase gate for two different tunneling couplings t in μeV. (b) Visibility (full line) and corresponding von-Neumann entropy (dashed line) as a function of the tunnel coupling.

In Fig. 2 (a) and (b), we show the results of our 3D 2-particle Green's function calculation of the ballistic current through the entangled QWR-DQD system. Fig. 2(a) shows the currents J_0 and J_1 as a function of V_G for two different values of the tunnel coupling. In both cases, the currents J_0 and J_1 show an oscillatory pattern. However, in the case of non-vanishing tunnel coupling, the visibility of the interference gets strongly suppressed. Fig. 2(b) shows the visibility and the corresponding von-Neumann entropy at $V_G = 0$ as a function of the tunnel coupling which quantifies the degree of entanglement of the QWR and the DQD subsystems.

References

1. Loss, D. and Sukhorukov E. V.: *Phys. Rev. Lett.*, **84**, 1035, 1998.
2. Reina J. H., Quiroga, L., Johnson, N. F.: *Phys. Rev. A*, **62**, 012305, 2000.
3. Ionicioiu, R., Zanardi, P., and Rossi, F.: *Phys. Rev. A*, **63**, 050101, 2001.
4. Cerletti V., Coish, W. A. Gywat O., Loss, D., *Nanotechnology*, **16**, R27, 2005.
5. Krenner H. J., Stufler S., Sabathil M., Clark, E. C., Ester, P., Bichler M., Abstreiter G., Finley J. J., and Zrenner A.: e-print cond-mat/0505731.
6. Bertoni, A., Bordone, P., Brunetti, R., Jacoboni C., and Reggiani S., *Phys. Rev. Lett.* **84**, 5912 (2000).
7. Akguc, G. B., Reichl, L. E., Shaji, A., and Snyder, M. G.: *Phys. Rev. A*, **69**, 042303, 2004.
8. Sabathil, M., Mamaluy, D., and Vogl, P.: *Semicond. Sci. Technol.*, **19**, S137, 2004.
9. van der Wiel, W. G., De Franceschi, S., Elzerman, J. M., Fujisawa T., Tarucha, S., and Kouwenhoven, L. P.: *Rev. Mod. Phys.*, **75**, 1, 2003.
10. Mamaluy, D., Sabathil, M., and Vogl P.: *J. Appl. Phys.*, **93**, 4628, 2003.

Simulation of Entanglement Creation for Carrier-Impurity Scattering in a 2D System

P. Bordone and A. Bertoni

National Research Center S3, INFM-CNR , and Dipartimento di Fisica, Università di Modena e Reggio Emilia, via Campi 213/A, I-41100, Modena, Italy.

Summary. We present a time dependent numerical analysis of the entanglement created between an electron freely propagating in a 2D system and a charged particle bound to a specific site by a harmonic potential. The latter can be considered as a simplified model of a shallow impurity. The dynamics of the carrier initially bound in the harmonic potential is coupled to that of the incoming electron through a screened Coulomb interaction. The entanglement is found to depend significantly on the energy of the freely propagating particle, on the confining energy of the harmonic potential and on the sign of the charge bound by the harmonic potential. This approach allows a quantitative estimate of the decoherence undergone by a propagating carrier due to a single unelastic scattering.

1 Introduction

The decoherence of a quantum system is ascribed to its entanglement with another system considered as the environment [1], thus the quantitative evaluation of entanglement formation dynamics can shed light on the transition between quantum and classical behavior of a carrier that undergoes a scattering event. It is then crucial to quantify the amount of decoherence suffered by a carrier when it interacts, unelastically, with phonons, impurities or other carriers. In each of these cases the carrier gets entangled with the scatterer thus making impossible to continue to describe it by means of a single particle wavefunction. As a consequence if the final quantum state of the scatterer, considered as part of the environment, is unknown, the carrier loses its quantum coherence.

We present a time dependent numerical analysis of the scattering process that creates entanglement between an electron freely propagating in a 2D system and a charged particle bound to a specific site by a harmonic poten-